High quality-factor label-free single analyte detection with MEMS cantilevers integrated into microfluidic systems

Journal:	*Analytical Chemistry*
Manuscript ID	ac-2017-011748.R3
Manuscript Type:	Article
Date Submitted by the Author:	06-Oct-2017
Complete List of Authors:	Kartanas, Tadas; University of Cambridge Department of Chemistry, Department of Chemistry Ostanin, Victor; University of Cambridge, Department of Chemistry Challa, Pavan Kumar; University of Cambridge, Chemistry Daly, Ronan; University of Cambridge, Engineering Charmet, Jerome; University of Warwick, WMG Knowles, Tuomas; University of Cambridge Department of Chemistry, Chemistry

High quality-factor label-free single analyte detection with MEMS cantilevers integrated into microfluidic systems

Tadas Kartanas[1,2], Victor Ostanin[1], Pavan Kumar Challa[1], Ronan Daly*[2], Jerome Charmet*[3,1] and Tuomas P.J. Knowles*[1,4]

[1]Department of Chemistry, University of Cambridge, Lensfield Road, Cambridge CB2 1EW, United Kingdom
[2]Department of Engineering, University of Cambridge, 17 Charles Babbage Road, Cambridge CB3 0FS, United Kingdom
[3]Institute of Digital Healthcare, WMG, University of Warwick, Coventry CV4 7AL, United Kingdom
[4]Cavendish Laboratory, University of Cambridge, J J Thomson Avenue, Cambridge CB3 0HE, United Kingdom
E-mail: rd439@eng.cam.ac.uk; J.Charmet@warwick.ac.uk; tpjk2@cam.ac.uk
Phone: +44 (0) 1223 7 66065; +44 (0) 24 7657 3566; +44 (0) 1223 336300

Abstract

Microelectromechanical systems (MEMS) have enabled the development of a new generation of sensor platforms. Acoustic sensor operation in liquid, the native environment of biomolecules, causes, however, significant degradation of sensing performance due to viscous drag and relies on the availability of capture molecules to bind analytes of interest to the sensor surface. Here we describe a strategy to interface MEMS sensors with microfluidic platforms through an aerosol spray. Our sensing platform comprises a microfluidic spray nozzle and a micro-cantilever array operated in dynamic mode within a closed loop oscillator. A solution containing the analyte is sprayed uniformly through pico-litre droplets onto the micro-cantilever surface; the micron-scale drops evaporate rapidly and leave the solutes behind, adding to the mass of the cantilever. This sensing scheme results in a 50-fold increase in the quality factor compared to operation in liquid, yet allows the analytes to be introduced into the sensing system from a solution phase. It achieves a 370 femtogram limit of detection and we demonstrate quantitative label-free analysis of inorganic salts and model proteins. These results demonstrate that the standard resolution limits of cantilever sensing in dynamic mode can be overcome with the integration of spray microfluidics with MEMS.

Introduction

The development of platforms for biosensing has been the subject of extensive research efforts for a number of years. However, fundamental challenges remain in developing devices to meet the need for sensitive, quantitative and high-throughput[1] sensing which is required to unlock many key applications including in vitro diagnostics[2]. Micro-electromechanical systems (MEMS), which can be mass produced and fully integrated with microelectronics, are promising candidates for low cost, high resolution gravimetric biosensing[3,4]. However, even though they can reach resolutions down to the zeptogram under high vacuum conditions[5], such transducers suffer high losses when operated in a viscous liquid environment, degrading their gravimetric sensitivity and reducing the quality factor[6–9]. Indeed, using a first order approximation and neglecting changes in the material stiffness upon analyte adsorption, the sensitivity is given by:

$$\frac{\Delta f}{\Delta m} = -\frac{f_0}{2m_0} \#(1)$$

where m_0 is the effective mass and f_0 is the resonant frequency of the resonator. Using this simple equation, the changes in the resonant frequency Δf can be related to the mass changes Δm on the surface of the resonator. High sensitivity can thus be achieved by reducing the transducer size to minimise its mass and maximise the resonant frequency. The quality factor Q is an important measure directly related to the sensor limit of detection (LOD), as it quantifies the sharpness of the resonance peak and sets a limit on the minimum detectable frequency shift. The typical quality factor of MEMS sensors in vacuum[10,11] can be as high as 10^4-10^6 whereas it drops down to 100-1000[12,13] in air and can be lower than 10 in liquids[14–17]. This low Q-factor, which causes a wider resonance peak, significantly limits the minimum detectable mass of the sensor. Moreover, the effective mass of the resonator increases in liquids, thus, further reducing the transducer sensitivity[9,18]. Finally, the interpretation of the sensor readouts in liquid is not straightforward as the frequency shifts are caused by both the gravimetric loading and the increased viscous drag[6].

Another technical barrier potentially frustrating the more widespread entry of micro/nano sized sensors into the market as bio-sensors[19] is their problematic integration with sample delivery and preparation techniques using small sample volumes[3,20,21]. A

commonly used approach to address the integration challenge is to functionalise the resonator surface with capture molecules[22], which target specific proteins, and measure the resonator frequency shifts in liquid flow cells. This approach leads to a number of possible issues. In particular, the surface capture molecule design is a complex and costly process and many key disease biomarkers, for example for Alzheimer's disease[23,24], still need specific labels to be developed. In the case of conventional biosensing, including Surface Plasmon Resonance (SPR)[25] and quartz crystal microbalance (QCM) flow cells[26,27], standard capture molecules are required and the presence of a surface can influence the measured affinity values and, hence, the mass measurements. Moreover, the flow cell needs a careful design taking into account the analyte diffusion and convection towards the sensor; this optimisation is needed to maximise the reaction rate between the capture molecules and the biomarker[28].

A particularly innovative and elegant solution to address MEMS sensor integration and Q-factor losses when operating in liquid is to integrate a narrow channel inside the cantilever[29] and measure the buoyant mass of the analytes that flow through the channel. Such suspended nanochannel resonators have enabled the measurement of masses down to the attogram scale in liquid[30,31], and more recently have achieved an increased throughput[32]. However, their fabrication still remains complex and the setup requires a vacuum package to minimize viscous losses[8].

Here we explore a fundamentally different approach to high Q-factor sensing of analytes in liquids by spraying droplets onto a gravimetric sensor using microfluidics (Figure 1). The micron-scale droplets evaporate rapidly leaving the dry solute on the sensor surface and thereby decreasing its resonant frequency. The relationship between the increased mass of the sensor and the frequency shift is given by equation 1. This detection scheme in air is designed to suffer less from the decrease in the sensor resolution due to the viscous losses inherent to measurements in liquid[6]. To explore the potential of this approach we have built an AFM-like[33] MEMS cantilever resonant frequency measurement setup and integrated it with a 3D microfluidic spray fabricated for the purpose of the study using soft lithography techniques[34]. The spray nozzles work by creating Rayleigh-Taylor type of instability[35] with the help of pressurised gas flowing past a narrow fluid outlet. Similar nozzles were previously used for drug formulation[36], microbubble generation[37] and amorphous nanoparticle production[38].

Dry mass sensing in air is on a conceptual level a tightly controlled and thus more robust version of one of the earliest biosensing dip-dry-measure formats[39]. It is compatible with many gravimetric sensors and could enable for label-free detection of molecules at extremely low concentrations. The sensing principle has already been demonstrated to give nanogram scale detection with a QCM[40]. Our work uses MEMS cantilevers as alternative sensors which allows us to achieve a 3 orders of magnitude lower LOD in air, 370 femtogram. Since the spray nozzle is based on lithography-enabled microfluidic fabrication techniques[21], the integration of upstream microfluidic separation[41–43], mixing[44] or filtering[45] is a suitable route to allow for selective analyte detection. More generally, dry mass sensing could be used in laboratory settings for the concentration measurements of single analytes replacing or complementing ultraviolet-visible light (UV-Vis) spectrometers that are typically limited to a concentration of few micro-grams per millilitre and very molecule dependent. It will potentially be a very useful complementary tool to protein sensing techniques exploiting optical[46], biochemical and electrochemical phenomena[47,48]. This work to our

knowledge is the first attempt combining the benefits of microscale flow processing with MEMS high Q-factor in-air measurement.

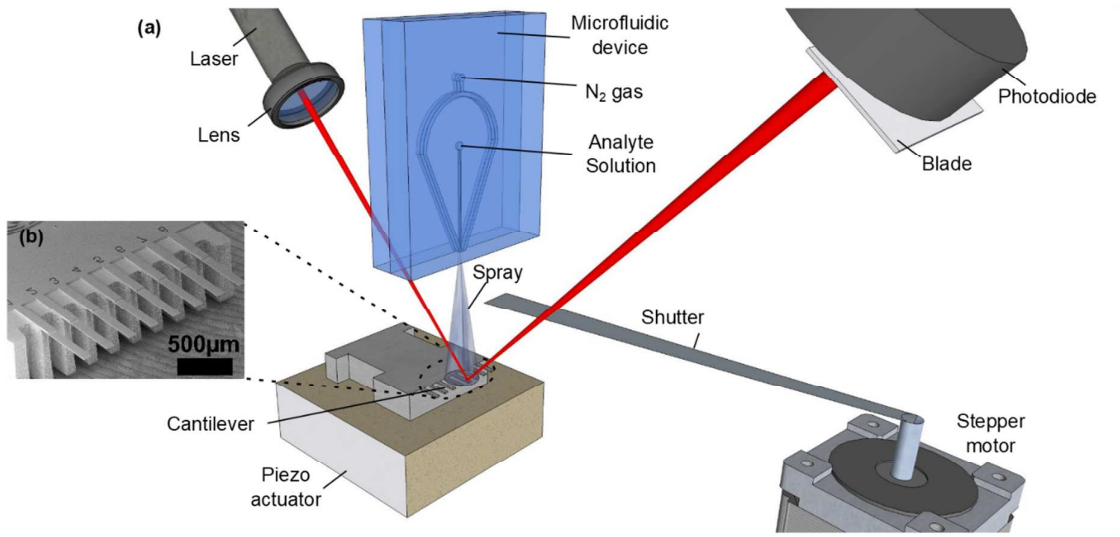

***Figure 1**: (a) A scheme of the dry mass sensing setup. A 3D microfluidic spray nozzle, positioned above a MEMS sensor (SEM image shown in (b)), uniformly sprays micrometer-sized rapidly evaporating droplets to the cantilevers, thus, gradually increasing the sensor mass and decreasing its resonant frequency. A laser beam is focused onto a MEMS cantilever which is in turn excited by a piezo ceramic actuator. The resulting motion of the laser beam is detected with a single channel photodiode. The shutter stops the spray, the cantilever is locked in the lowest transverse oscillation mode with a positive feedback loop and the resonant frequency is measured with a frequency counter reading the time-dependent signal from the photodiode.*

Experimental Section

In brief, we designed a microfluidic device to generate a micrometer-sized liquid spray; the device is used to deposit accurate amounts of analyte solution onto a MEMS cantilever. The cantilever resonant frequency is monitored using a custom built optical system within a positive feedback loop circuit[33]. A shutter periodically stopping the spray allows a stable cantilever frequency readout. The analytes dry uniformly on the cantilever surface, increasing its mass and, hence, a decrease in the resonant frequency of the cantilever over time is observed.

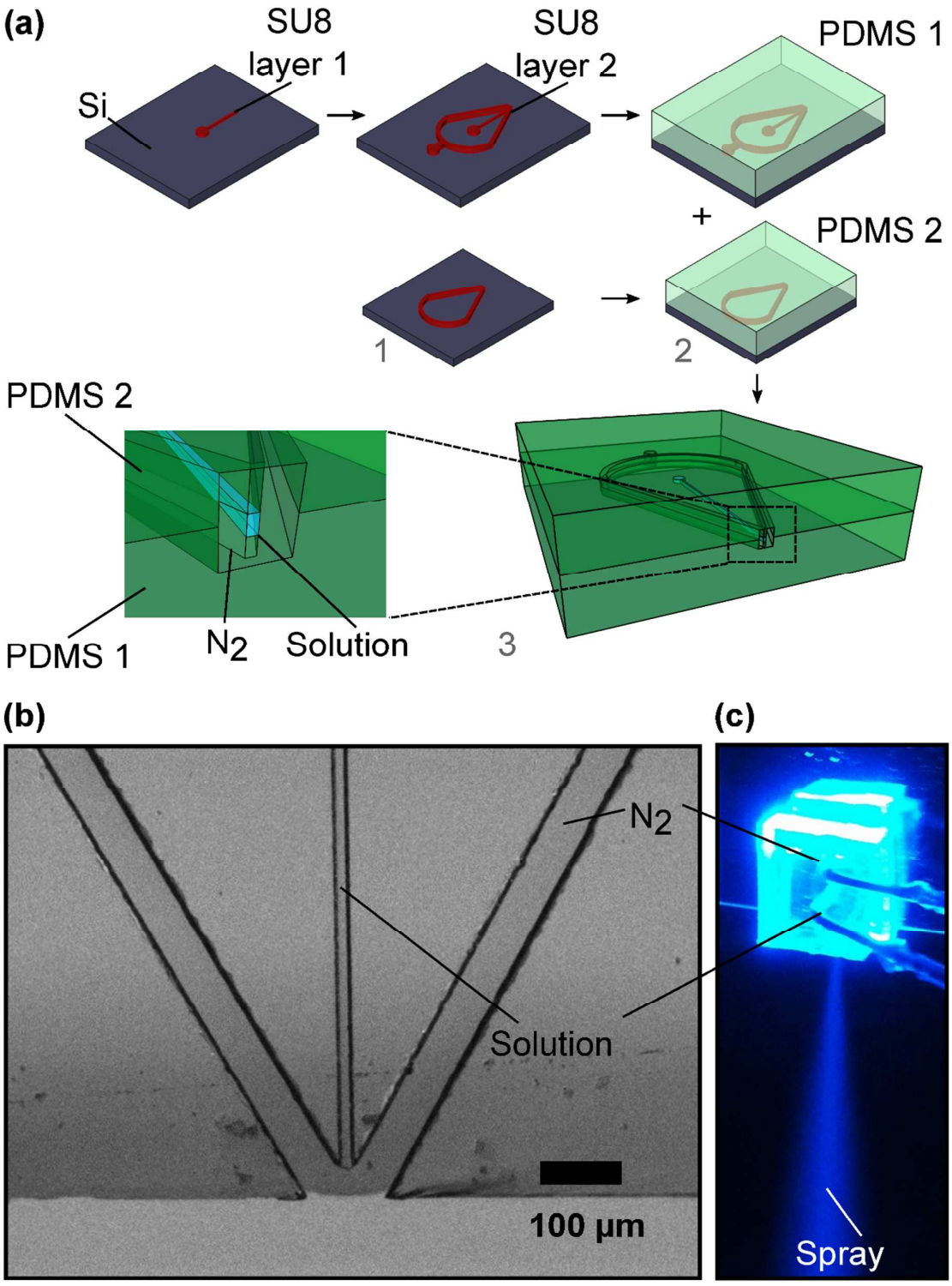

Figure 2: *The 3D microfluidic spray nozzle. The liquid droplets are generated at the device outlet where the fluid channel is surrounded by gas flow from all directions. (a) The general fabrication steps consist of two-layer photolithography (step 1), soft-lithography of two parts (step 2) and assembly (step 3). (b) An optical image of the spray nozzle which has two inlets: one for a liquid to be sprayed and another for an inert gas. (c) A picture taken during the continuous device operation.*

Microfluidic spray

The devices were fabricated using a standard polydimetylsiloxane (PMDS) soft-lithography approach[49,50]; the masters for the replica moulding of PDMS were produced with a 2 step SU-8 photolithography process as shown in Figure 2a. The first master consists of a two-mask design comprising a 20 µm x 25 µm solution channel and a second layer with 50 µm x 100 µm channels for the gas. The second master has only the gas channels. After mixing PDMS (Sylgard184, Dow Corning - two components mixed 10:1 ratio and degassed) and casting it onto the lithography masters, it is cured at 70^0 C for 3 hours. The PDMS replica of each master is then cut and the connection holes were formed with the help of a biopsy punch. The PDMS parts were sonicated for 3 minutes in isopropanol, blow dried with N_2 and placed in an oven at 70^0 C for 10 min. The two PDMS elements were then activated using O_2 plasma (Diener etcher, Femto, 40 % power, 30 s and put in contact with each other, after a drop of methanol had been deposited on one of the surfaces. The methanol was used to give enough time before the bonding takes place to position the features precisely[51,52] such that the two gas transporting channels are aligned. The PDMS device was then cut at the nozzle outlet with a razor blade. Finally, the sealed chips were plasma bonded to a clean glass slide and are ready to use. Figure 2b shows an optical image of the fabricated devices. A controlled flow of 50-150 µL/h rates was driven through the solution inlet using a syringe pump (Harvard Apparatus PHD2000). The other inlet was connected to a 2 bar pressure source from a pressurised N_2 cylinder resulting in a fine droplet spray cone of few millimetres in width (Figure 2c).

MEMS cantilevers

The resonant frequency of a cantilever in vacuum is given by:

$$f_n = \frac{\alpha_n^2}{2\pi}\sqrt{\frac{EH}{12\rho L^4}} \#(2)$$

where $\alpha_n$is the n-th excitation mode shape constant, E is the Young modulus, ρ – the density, H – the thickness and L is the length of the cantilever[53]. Silicon OCTOSENSIS dynamic mode cantilevers containing eight cantilevers per chip were purchased from Micromotive MIKROTECHNIK (see Figure 1b). The cantilever dimensions are L = 500 ± 4 µm, W = 90 ± 2 µm, H = 5 ± 0.3 µm with the errors indicating manufacturing process tolerances. For a cantilever operating in the first mode (α_0= 1:875, E = 180 GPa, ρ = 2330 kg/m^3), the resulting prediction for the mass is m_0 = 524 ± 34 ng and the resonant frequency f_0 = 28:4 ± 1:8 kHz after combining the errors of the physical cantilever size in quadrature. In order to account for the difference in the resonant frequency of each resonator due to manufacturing uncertainties, the resonant frequency of each sensor was measured prior to every experiment and their mass is estimated as described in Supporting Information.

Sensing platform

A scheme of the sensor platform is shown in Figure 1. The cantilevers are excited with a piezo ceramic actuator from ThorLabs (TA0505D024W). The cantilever chip is clamped to the piezo actuator which is in turn fixed to an xyz-micrometer stage. A 1 mW (635 nm) laser beam is focused on the cantilever surface; the position of reflected beam is detected with a single channel photodiode from ThorLabs (SM1PD1A) with a half of the beam covered. The cantilever oscillation results in the variation of the reflected beam position and, therefore,

the exposed area on the photodiode. This arrangement consisting of a single photodiode is significantly simpler than the multi-quadrant photodiode setups conventionally used for this purpose. In addition, an analog feedback loop was implemented to keep the chosen cantilever oscillating at its resonant frequency. The frequency was recorded with a frequency counter (TTi TF930) using 1s running average and the continuous frequency measurement data acquisition was monitored by a Raspberry Pi 2. More details about the positive feedback loop and pictures of the setup are presented in Figures S-1 and S-2 in the Supporting Information.

Shutter and frequency extraction

Spraying onto a cantilever surface introduces instabilities due to the droplets landing and evaporating on the surface as well as perturbations from the nitrogen flow. These factors together mean that the resonant frequency cannot be recorded accurately during continuous spraying. Therefore, a remotely controlled mechanical shutter actuated using a stepper motor was included to stop the spray for 5 s, allowing stable frequency readouts to be acquired during the closed interval. The analyte was sprayed onto the cantilevers for 45 s (90 % of the time). Typically, three to four frequency points were measured before the shutter was opened allowing the spray to come into contact with the sensor and the last reading was chosen as the frequency point (Figure S-3, Supporting Information).

Analyte solutions

NaCl salt (Fisher Scientific), bovine serum albumin (BSA) (Sigma-Aldrich, A7906) and lysozyme (Sigma-Aldrich, L6876) protein solutions were selected as representative analytes and used to perform the mass sensing experiments. The aqueous solutions were prepared with 18 M-Ohm desalinated water from PureLab Maxima. In the case of BSA and lysozyme, the sample was filtered with a 0.2 µm filter and the concentration is measured with Nanodrop 2000 UV-Vis Spectrophotometer.

Response curve and phase noise measurements

The cantilever chip is fixed to the piezo actuator and is placed in a closed chamber with a transparent window for the laser beam. The resonator response curve and the feedback loop phase noise[54], which describes qualitatively the noise level in the system, are measured in air and water. For the measurements in liquid, the chamber is filled with deionised water. The laser beam position is adjusted with the micrometer stage to account for the change in the refractive index. The resonator is tested in an open loop configuration using a lock-in amplifier SR830 from Stanford Research Systems (Figure S-5, Supporting Information). For the response curve measurements, scans around the resonant frequency in steps of 10 Hz are performed using 100 ms time constant. Then the resonant cantilever frequency is selected and the loop phase variation over time is measured using 1 s time constant to match it with the frequency counter time constant.

Results and discussion

System characterisation

The Q-factor is the main parameter determining the limit of detection (LOD) of an acoustic resonator. In this section, we present the characteristics of the sensing platform and

evaluate the advantage of the operation in air versus water. We have determined the MEMS cantilever LOD in air by evaluating the cantilever frequency variation over time.

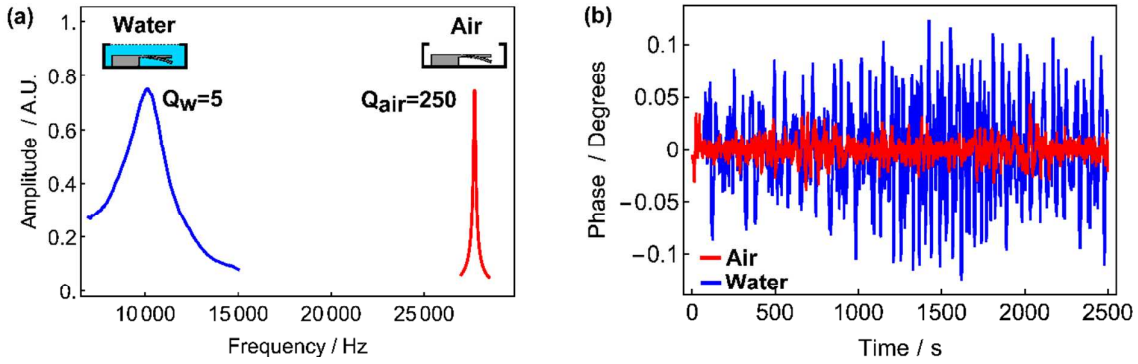

Figure 3: *The cantilever resonance characteristics in water and air. (a) Normalised cantilever response around resonance; the quality factor of the cantilevers was 250 in air compared to 5 in water leading to a much lower phase noise level in air (b).*

The sensor LOD, usually denoted as the minimum detectable added mass (Δm_{min}), is inversely proportional to the Q-factor[39]:

$$LOD = \Delta m_{min} \propto \frac{m_0}{Q} \#(3)$$

where m_0 is the mass of the empty resonator. The sensor platform is operated in air for 1 hour and the frequency is recorded with the frequency counter (Figure S-4, Supporting Information). The Allan deviation[55] with a gate time of 1 s gives 0.01 Hz frequency noise. The 0.01 Hz noise level in air corresponds to a 370 fg using equation (1) which is the ultimate sensor LOD in air.

To probe the advantages of operating the cantilevers in air, we measure the response curves and phase noise in water and air (Figure 3a). The quality factors are obtained by fitting the measurements (Figure S-6, Supporting Information) to the frequency response of an oscillator in the harmonic limit[13]:

$$A(\omega) = \frac{A_0 \omega_0^2}{\sqrt{(\omega^2 - \omega_0^2)^2 + \omega^2 \omega_0^2 Q^{-2}}} \#(4)$$

where, $\omega = 2\pi f$ is the angular driving frequency, A_0 is the amplitude of the response, Q is the quality factor, and $\omega_0 = 2\pi f_0$ corresponds to the cantilever resonant frequency. The Q-factors obtained are $Q_{water} \approx 5$ and $Q_{air} = 250$ respectively. The phase noise[54], which describes the system phase stability within a feedback loop at resonance, is also measured both in water and air (Figure 3b). The phase noise in water is $\Delta\varphi_{water} = 0.044^0$ and air $\Delta\varphi_{air} = 0.01^0$. The frequency noise can be expressed as follows:

$$\Delta f = \left(\frac{d\varphi}{df}\right)^{-1} \Delta\varphi \#(5)$$

where $d\varphi/df$ is a phase versus frequency gradient at resonance and $\Delta\varphi$ is the phase noise. Using the measured phase as a function of frequency gradients -73.3 mHz/s and -0.97 Hz/s for water and air respectively (Figure S-6, Supporting Information) the frequency noise is found to be 0.61 Hz and 0.01 Hz respectively. The ratio between the frequency noise levels is $\Delta f_{water}/\Delta f_{air} \approx 60$ and is very similar to the ratio of the quality factors ($Q_{air}/Q_{water} \approx 50$).

These results show that the mass sensing approach in air improves the LOD of the sensor by two orders of magnitude compared to operation in water[9,18].

Mass sensing experiments

We first demonstrate the ability to detect dry mass in saline solutions and select NaCl in deionised water as a test system. Then in a second step, to perform label-free protein sensing and focus on bovine serum albumin (BSA). We show that our measurement scheme yields a linear concentration response and, moreover, that the cantilever frequency decrease rate depends on the solution spraying rate. Further, we compare BSA concentration sensitivity with conventional UV absorption measurements and show that we achieve lower concentration protein detection . Finally, we show that the cantilever dry mass sensing can yield label-free quantitative concentration measurements with a calibration step before the measurement using a dual-inlet microfluidic spray device.

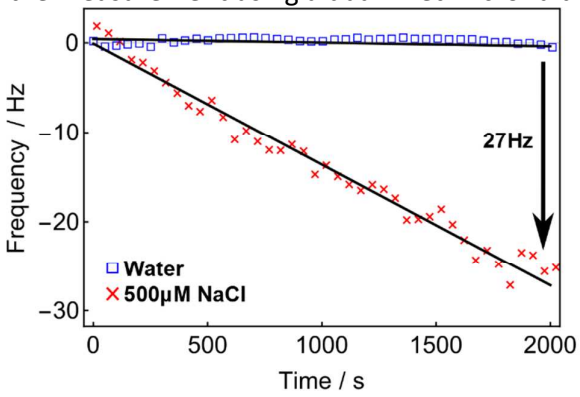

Figure 4: *Resonant frequency variation of the cantilever while spraying deionised water and NaCl solution. The frequency (referenced to 27734 Hz) decreases by 27 Hz over 2000 s as a result of spraying 500 µM NaCl salt on the sensor at a 50 µL/h flow rate.*

Mass calibration

We first spray deionised water on the MEMS cantilevers and confirm that it causes a negligible frequency change (Figure 4). The standard deviation of the frequency signal is measured to be 0.32 Hz over a 2000 s measurement. We then spray a 500 µM NaCl solution onto the cantilevers at a flow rate of 50 µL/h. We observe that the frequency decreases due to the dry mass of NaCl accumulating on the surface (Figure 4). The frequency trend gradient is evaluated and used to estimate the mass deposition rate. The frequency decrease by 27 ± 0.32 Hz over 2000 s thus corresponds to a salt mass of 1.00 ± 0.03 ng deposited on the cantilever. The mass deposited on the sensor during one 45 s spraying interval is 24.9 ± 0.8 pg. In order to verify the masses obtained using the frequency measurements, we compare the values with the estimates based on the total amount of salt sprayed. Throughout 45 s the total NaCl amount released by the microfluidic spray device is 18.3 ng but only a fraction of the liquid is captured on the cantilevers: the spray diameter is 6.5 ± 0.5 mm at the cantilever level 2 cm away from the spray, whereas the area of a single cantilever is A_c = 45000 µm^2. Taking this factor into consideration, the total mass reaching the sensor corresponds to 25 ± 4 pg which agrees with the measured value within the errors.

Sensing BSA at different concentrations

We next verify that this approach can be applied to determine the dry mass of proteins in aqueous solution. To this effect, we prepare 100 nM and 500 nM BSA protein solutions and spray them on a cantilever at a 50 µL/h flow rate (Figure 5a). First, we observe that the fluctuations in the frequency are further reduced for the BSA solution compared to NaCl experiments. This finding may be explained by the fact that BSA adheres to surfaces at neutral pH conditions[56] and, therefore, protein molecules already deposited on the cantilever are not displaced by the droplets landing subsequently. In the case of NaCl, the droplets landing on the cantilever may dissolve and displace the salt crystals deposited previously. The 100 nM solution gives a -3.2 mHz/s decrease gradient whereas it is -18.3 mHz/s for the 500 nM solution. We also spray deionised water to determine the error in the gradients for the continuous mass sensing experiments and obtain a trend with a gradient of -0.4 mHz/s. As expected the 500 nM protein solution gives a steeper frequency drop with a ratio between the two different concentrations 5.8 ± 0.8 taking into account the error in gradient while spraying water. The experimental procedure might have introduced some systematic errors: two different spray nozzles are used and the alignment of the nozzles above the sensors is a little different. However, these errors are not significant and only a small variation from the expected ratio of 5 is observed.

Sensing BSA at different flow rates

Next, we explore whether it is possible to deliver the analytes on the sensor at different volumetric flow rates. To demonstrate this objective 100 nM BSA solution is sprayed at multiple flow rates: 50 µL/h, 100 µL/h and 150 µL/h. Our data in Figure 5b shows that indeed the frequency shift is related to the liquid spray rate. The measured gradients are -3.9 ± 0.4 mHz/s, -9.4 ± 0.4 mHz/s and -16:8 ± 0.4 mHz/s respectively giving ratios 1:2.4:4.3. The small difference from the expected result 1:2:3 is likely to arise from the fact that the spray angle and thus the droplet density distribution within the spray area changes slightly at different flow rates. We note that this behaviour is not an obstacle for mass sensing with a fixed flow rate since the spray area remains constant.

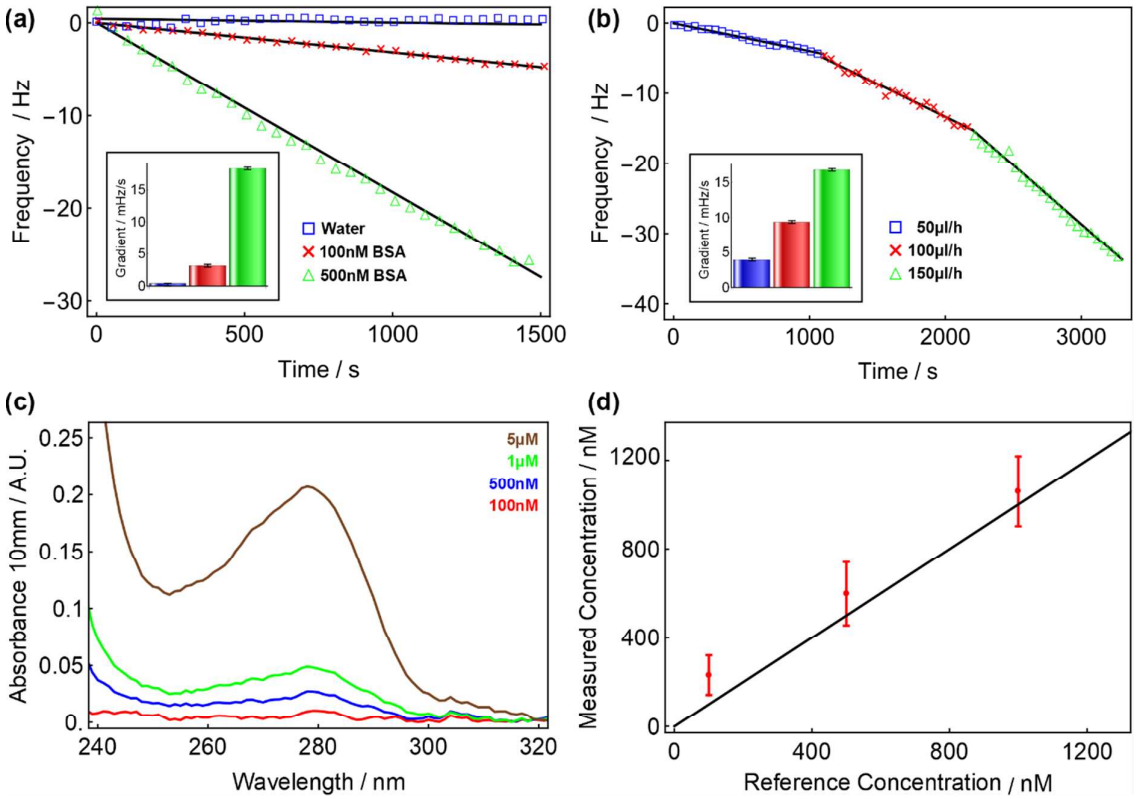

Figure 5: *Frequency shift induced by the deposition of BSA. (a) shows the comparison between deionised water and BSA at different concentration and fixed flow rate of 50 µL/h (start frequency 27165 Hz). (b) depicts the frequency downshift induced by a 100 nM BSA solution sprayed at different flow rates (start frequency 27132 Hz). (c) shows the UV absorption spectra of BSA for different concentrations using NanoDrop 2000 and (d) illustrates the concentration measurement of dilute BSA solutions based on absorption value at 280 nm.*

BSA concentration measurement with UV absorption

To compare our results with conventional quantification by UV absorption, we measured UV absorption spectra of BSA at different concentrations ranging from 100 nM to 5 µM with NanoDrop 2000 (Figure 5c). Absorption values (see Table S-1 in Supporting Information) at 280 nm using a 10mm optical path show that NanoDrop 2000 performs well down to 1 µM whereas the measurement is less accurate at lower concentrations. The measured concentrations of 100 nM and 500 nM BSA solutions are 230 ± 100 nM and 600 ± 160 nM. The error bars depict the variation in the estimated concentration obtained from ten UV absorption measurement repeats (Figure 5d).

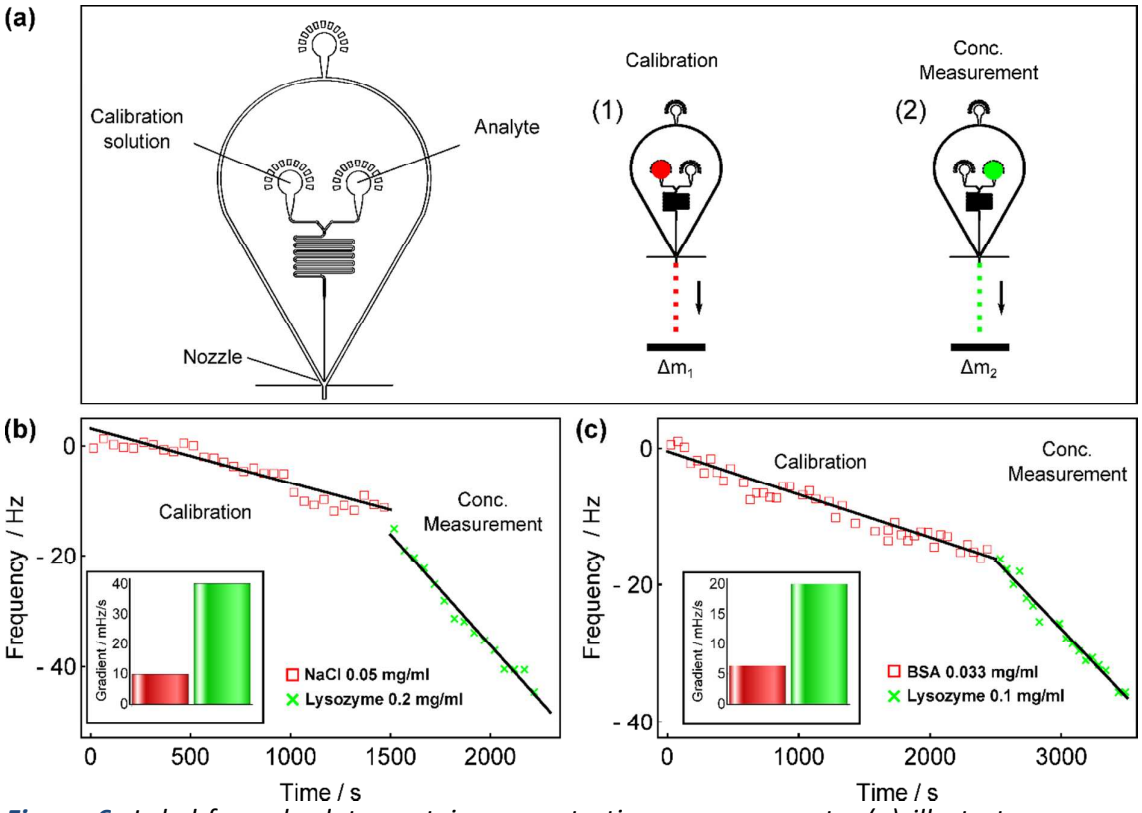

Figure 6: *Label-free absolute protein concentration measurements. (a) illustrates a spray device designed for the experiment and the measurement scheme.(b) shows 0.2 mg/ml lysozyme concentration measurement; the calibration step is performed with 0.05 mg/ml NaCl solution. (c) depicts the calibration step performed with 0.033 mg/ml BSA followed by a 0.1 mg/ml lysozyme solution concentration measurement.*

Lysozyme concentration measurements with calibration

Finally, we perform absolute protein concentration measurements in a label-free manner. For this purpose, we design and fabricate a microfluidic spray device with two inlets allowing for the co-spray of two fluids (see Figure 6a). A calibration step is readily implemented into the system by first spraying a known concentration solution on a cantilever, recording the deposition gradient, and then repeating the experiment with the analyte of interest without changing the spray alignment. First, we perform the experiment with a 0.05 mg/ml NaCl calibration step followed by 0.2 mg/ml lysozyme deposition (see Figure 6b). The measured gradients are -9:76 ± 0.4 mHz/s and -40:1 ± 0.4 mHz/s respectively giving ratio 1 : 4.11 and the concentration estimate of 0.205 mg/ml. Further, we perform a similar experiment but instead using 0.033 mg/ml BSA solution for calibration followed by 0.1 mg/ml lysozyme (see Figure 6c). The measured gradients are -6:31 ± 0.4 mHz/s and -20:0 ± 0.4 mHz/s giving the ratio 1 : 3.17 and the concentration estimate of 0.105 mg/ml. These experiments demonstrate that dry mass sensing is not only a very sensitive label-free single analyte detection technique but also can yield accurate concentration measurements.

Conclusions

This work presents a path to address limitations to MEMS biosensing originating from low quality factor of micro/nano acoustic resonators operated in liquids[6]. The resonant

frequency measurement system of a MEMS cantilever is built and combined with a 3D microfluidic spray nozzle delivering rapidly evaporating droplets to the cantilever surface. The dry mass of the solute deposited on the surface after the evaporation can be calculated by measuring the decrease in the sensor resonant frequency. The system is a demonstration of a flexible interface between the current state of art microfluidics and MEMS devices.

The dry mass sensing approach allows us to improve the quality factor by two orders of magnitude relative to operation in liquid leading to a 370 fg gravimetric limit of detection. We demonstrate mass sensing with 500 µM NaCl solution measuring a mass of 24.9 ± 0.8 pg during a 45 s interval. Moreover, we show with 100 nM and 500 nM BSA protein solutions that this label-free mass detection principle is also sensitive to the analyte concentration as well as the sample delivery rate to the MEMS surface. Finally, dry sensing can be used to determine the mass concentration of a single analyte solution by performing a calibration step with a sample of known concentration.

The sensing scheme presented is in principle compatible with a wide range of gravimetric sensors and, therefore, opens up new perspectives for high resolution biosensing using ultra-sensitive micro/nano-mechanical sensors. The full potential of this measurement strategy using complex analyte mixtures can leverage microfluidic upstream protein separation techniques such as diffusive filtering[45,57] and free-flow electrophoresis[41–43]. We expect this versatile system to have numerous applications including analysis of sample of unknown concentration as well as offer other novel possibilities for label-free sensing community.

Acknowledgement

The research leading to these results has received funding from the European Research Council under the European Union's Seventh Framework Programme (FP7/2007-2013) through the ERC grant PhysProt (agreement n° 337969). We gratefully acknowledge financial support from the Engineering and Physical Sciences Research Council (EPSRC) and Frances and Augustus Newman Foundation. We also acknowledge support from the Nanotechnologies Doctoral Training Centre in Cambridge (NanoDTC Cambridge EP/L015978/1). We finally acknowledge the Cambridge Advanced Imaging Centre for help with the SEM imaging.

Supporting Information Available

Setup pictures, exact schematics with the positive feedback loop electronic components, cantilever resonant frequency error estimation, system stability, and frequency response curves around resonance. This material is available free of charge via the Internet at http://pubs.acs.org.

References

(1) Hong, J.; Edel, J. B.; DeMello, A. J. *Drug Discov. Today* **2009**, *14*, 134–146.
(2) Ahmed, M. U.; Saaem, I.; Wu, P. C.; Brown, A. S. *Crit. Rev. Biotechnol.* **2014**, *34*, 180–196.
(3) Arlett, J. L.; Myers, E. B.; Roukes, M. L. *Nat. Nanotechnol.* **2011**, *6*, 203–215.
(4) Bridle, H.; Wang, W.; Gavriilidou, D.; Amalou, F.; Hand, D. P.; Shu, W. *Sensors Actuators A Phys.* **2016**, *247*, 144–149.
(5) Yang, Y. T.; Callegari, C.; Feng, X. L.; Ekinci, K. L.; Roukes, M. L. *Nano Lett.* **2006**, *6*, 583–586.
(6) Lucklum, R.; Hauptmann, P. *Anal. Bioanal. Chem.* **2006**, *384*, 667–682.
(7) Dufour, I.; Lemaire, E.; Caillard, B.; Debéda, H.; Lucat, C.; Heinrich, S. M.; Josse, F.; Brand, O. *Sensors Actuators B Chem.* **2014**, *192*, 664–672.

(8) Vančura, C.; Dufour, I.; Heinrich, S. M.; Josse, F.; Hierlemann, A. *Sensors Actuators A Phys.* **2008**, *141*, 43–51.
(9) Waggoner, P. S.; Tan, C. P.; Bellan, L.; Craighead, H. G. *J. Appl. Phys.* **2009**, *105*, 94315.
(10) Kaajakari, V.; Mattila, T.; Oja, A.; Kiihamaki, J.; Seppa, H. *IEEE Electron Device Lett.* **2004**, *25*, 173–175.
(11) Abdolvand, R.; Johari, H.; Ho, G. K.; Erbil, A.; Ayazi, F. *J. Microelectromechanical Syst.* **2006**, *15*, 471–478.
(12) Verbridge, S. S.; Ilic, R.; Craighead, H. G.; Parpia, J. M. *Appl. Phys. Lett.* **2008**, *93*, 13101.
(13) Chon, J. W. M.; Mulvaney, P.; Sader, J. E. *J. Appl. Phys.* **2000**, *87*, 3978–3988.
(14) Kwon, T. Y.; Eom, K.; Park, J. H.; Yoon, D. S.; Kim, T. S.; Lee, H. L. *Appl. Phys. Lett.* **2007**, *90*, 223903.
(15) Verbridge, S. S.; Bellan, L. M.; Parpia, J. M.; Craighead, H. G. *Nano Lett.* **2006**, *6*, 2109–2114.
(16) Ramos, D.; Tamayo, J.; Mertens, J.; Calleja, M. *J. Appl. Phys.* **2006**, *99*, 124904.
(17) Vančura, C.; Lichtenberg, J.; Hierlemann, A.; Josse, F. *Appl. Phys. Lett.* **2005**, *87*, 162510.
(18) Maali, A.; Hurth, C.; Boisgard, R.; Jai, C.; Cohen-Bouhacina, T.; Aimé, J.-P. *J. Appl. Phys.* **2005**, *97*, 74907.
(19) Menon, K.; Joy, R. A.; Sood, N.; Mittal, R. K. *Bionanoscience* **2013**, *3*, 356–366.
(20) Wu, J.; Gu, M. *J. Biomed. Opt.* **2011**, *16*, 80901.
(21) Whitesides, G. M. *Nature* **2006**, *442*, 368.
(22) Onen, O.; Ahmad, A. A.; Guldiken, R.; Gallant, N. D. *Sensors* **2012**, *12*, 12317–12328.
(23) Fiandaca, M. S.; Mapstone, M. E.; Cheema, A. K.; Federoff, H. J. *Alzheimer's Dement.* **2014**, *10*, S196--S212.
(24) Andreasen, M.; Lorenzen, N.; Otzen, D. *Biochim. Biophys. Acta (BBA)-Biomembranes* **2015**, *1848*, 1897–1907.
(25) Homola, J.; Yee, S. S.; Gauglitz, G. *Sensors Actuators B Chem.* **1999**, *54*, 3–15.
(26) Cheng, C. I.; Chang, Y.-P.; Chu, Y.-H. *Chem. Soc. Rev.* **2012**, *41*, 1947–1971.
(27) Speight, R. E.; Cooper, M. A. *J. Mol. Recognit.* **2012**, *25*, 451–473.
(28) Squires, T. M.; Messinger, R. J.; Manalis, S. R. *Nat. Biotechnol.* **2008**, *26*, 417–426.
(29) Burg, T. P.; Godin, M.; Knudsen, S. M.; Shen, W.; Carlson, G.; Foster, J. S.; Babcock, K.; Manalis, S. R. *Nature* **2007**, *446*, 1066.
(30) Olcum, S.; Cermak, N.; Wasserman, S. C.; Christine, K. S.; Atsumi, H.; Payer, K. R.; Shen, W.; Lee, J.; Belcher, A. M.; Bhatia, S. N.; others. *Proc. Natl. Acad. Sci.* **2014**, *111*, 1310–1315.
(31) Modena, M. M.; Wang, Y.; Riedel, D.; Burg, T. P. *Lab Chip* **2014**, *14*, 342–350.
(32) Olcum, S.; Cermak, N.; Wasserman, S. C.; Manalis, S. R. *Nat. Commun.* **2015**, *6*.
(33) Okajima, T.; Sekiguchi, H.; Arakawa, H.; Ikai, A. *Appl. Surf. Sci.* **2003**, *210*, 68–72.
(34) Duffy, D. C.; McDonald, J. C.; Schueller, O. J. A.; Whitesides, G. M. *Anal. Chem.* **1998**, *70*, 4974–4984.
(35) Marmottant, P.; Villermaux, E. *J. Fluid Mech.* **2004**, *498*, 73–111.
(36) Thiele, J.; Windbergs, M.; Abate, A. R.; Trebbin, M.; Shum, H. C.; Förster, S.; Weitz, D. A. *Lab Chip* **2011**, *11*, 2362–2368.
(37) Peyman, S. A.; Abou-Saleh, R. H.; McLaughlan, J. R.; Ingram, N.; Johnson, B. R. G.; Critchley, K.; Freear, S.; Evans, J. A.; Markham, A. F.; Coletta, P. L.; others. *Lab Chip* **2012**, *12*, 4544–4552.
(38) Amstad, E.; Gopinadhan, M.; Holtze, C.; Osuji, C. O.; Brenner, M. P.; Spaepen, F.; Weitz, D. A. *Science (80-.).* **2015**, *349*, 956–960.
(39) Johnson, B. N.; Mutharasan, R. *Biosens. Bioelectron.* **2012**, *32*, 1–18.
(40) Müller, T.; White, D. A.; Knowles, T. P. J. *Appl. Phys. Lett.* **2014**, *105*, 214101.
(41) Herling, T. W.; Müller, T.; Rajah, L.; Skepper, J. N.; Vendruscolo, M.; Knowles, T. P. J. *Appl. Phys. Lett.* **2013**, *102*, 184102.
(42) Pamme, N. *Lab Chip* **2007**, *7*, 1644–1659.
(43) Lenshof, A.; Laurell, T. *Chem. Soc. Rev.* **2010**, *39*, 1203–1217.
(44) Thanh, N. T. K.; Green, L. A. W. *Nano Today* **2010**, *5*, 213–230.

(45) Brody, J. P.; Yager, P. *Sensors Actuators A Phys.* **1997**, *58*, 13–18.
(46) Celebrano, M.; Kukura, P.; Renn, A.; Sandoghdar, V. *Nat. Photonics* **2011**, *5*, 95–98.
(47) Yates, E. V; Müller, T.; Rajah, L.; De Genst, E. J.; Arosio, P.; Linse, S.; Vendruscolo, M.; Dobson, C. M.; Knowles, T. P. J. *Nat. Chem.* **2015**, *7*, 802.
(48) Arosio, P.; Müller, T.; Rajah, L.; Yates, E. V; Aprile, F. A.; Zhang, Y.; Cohen, S. I. A.; White, D. A.; Herling, T. W.; De Genst, E. J.; others. *ACS Nano* **2015**, *10*, 333–341.
(49) McDonald, J. C.; Whitesides, G. M. *Acc. Chem. Res.* **2002**, *35*, 491–499.
(50) Challa, P. K.; Kartanas, T.; Charmet, J.; Knowles, T. P. J. *Biomicrofluidics* **2017**, *11*, 14113.
(51) Jo, B.-H.; Van Lerberghe, L. M.; Motsegood, K. M.; Beebe, D. J. *J. microelectromechanical Syst.* **2000**, *9*, 76–81.
(52) Kim, J. Y.; Baek, J. Y.; Lee, K. A.; Lee, S. H. *Sensors Actuators A Phys.* **2005**, *119*, 593–598.
(53) Bonaccurso, E.; Butt, H.-J. *J. Phys. Chem. B* **2005**, *109*, 253–263.
(54) Robins, W. P. *Phase noise in signal sources: theory and applications*; IET, 1984; Vol. 9.
(55) Vig, J. R.; Kim, Y. *IEEE Trans. Ultrason. Ferroelectr. Freq. Control* **1999**, *46*, 1558–1565.
(56) Haskard, C. A.; Li-Chan, E. C. Y. *J. Agric. Food Chem.* **1998**, *46*, 2671–2677.
(57) Zhang, Y.; Buell, A. K.; Müller, T.; De Genst, E.; Benesch, J.; Dobson, C. M.; Knowles, T. P. J. *ChemBioChem* **2016**, *17*, 1920–1924.

Graphical TOC Entry